Acta Cryst. (1996). D**52**, 983–996

Growth Mechanism and Morphology of Tetragonal Lysozyme Crystals

ARUNAN NADARAJAH[a]* AND MARC L. PUSEY[b]

[a]*Department of Chemical and Materials Engineering, University of Alabama in Huntsville, Huntsville, Alabama 35899, USA, and* [b]*Biophysics Branch ES76, NASA/Marshall Space Flight Center, Huntsville, Alabama 35812, USA. E-mail: arun@lysozyme.eb.uah.edu*

(*Received 6 September 1995; accepted 2 April 1996*)

Abstract

The tetragonal form of hen egg-white lysozyme is the most investigated protein crystal for growth studies, but the relationship between its surface morphology and internal structure is still not well understood. One method of determining this relationship for inorganic crystals is by employing the periodic bond chain (PBC) theory of Hartman & Perdok [Hartman & Perdok (1955). *Acta Cryst.* **8**, 49–52, 521–524, 525–529]. However, complexities resulting from the packing arrangements and the number of intermolecular bonds in protein crystals have resulted in the use of only simplified versions of this theory so far. In this study a more complete PBC analysis of tetragonal lysozyme crystals was carried out, coupled with an approach incorporating the molecular orientations of the crystal structure. The analysis revealed the existence of a helical tetramer building block of the entire crystal structure, centered around the 4_3 crystallographic axes, resulting in double-layered slices and PBC's throughout. The analysis also indicated that the crystallizing units for the faces are at least as large as this tetramer, with the experimental evidence suggesting that it is a tetramer unit for the {101} faces and an octamer unit for the {110} faces. The {110} faces were shown to be molecularly smooth *F* faces, while the {101} to be essentially rough *S* faces. The predicted morphology and growth mechanisms were found to explain numerous experimental observations from electron and atomic force microscopy, etching studies, lysozyme aggregation studies and measurements of growth kinetics.

1. Introduction

In recent years there have been increased investigations of different model proteins for crystal growth studies, but hen egg-white lysozyme continues to be the one most studied. Among the crystal forms of lysozyme investigated, it is the tetragonal form that has received the most attention. Its crystallographic structure was first described by Phillips and coworkers (Blake *et al.*, 1965; Blake, Mair, North, Phillips & Sarma, 1967). Since then further studies have refined the structure and described the molecular packing arrangement and the hydration shell (Imoto, Johnson, North, Phillips & Rupley, 1972; Diamond, 1974; Moult *et al.*, 1976; Kodandapani, Suresh & Vijayan, 1990). However, the relationship between the surface morphology of the crystal and its internal structure is still not known with any certainty.

One method of determining this relationship involves the use of the periodic bond chain (PBC) theory of Hartman & Perdok (1955). This theory assumes that crystal growth proceeds by the formation of consecutive bonds between the crystallizing units (Hartman, 1987). It has mostly been used for predicting the habits of inorganic crystals, although lately it has been employed to predict phenomena such as roughening transitions (Bennema & van der Eerden, 1987; Bennema, 1993). The complexities of the intermolecular bonds between protein molecules and their packing arrangements in crystals makes the analyses of molecular packing in protein crystals a non-trivial task. This has resulted in some simplifications in the application of PBC theory to protein crystals. In one study crystals of a bacterial rubredoxin and of two scorpion neurotoxins were analyzed (Frey, Genovesio-Taverne & Fontecilla-Camps, 1988, 1992). The number of bonds and the size of the contact area between molecules were substituted for the interaction energy between them and simple spheres were used to represent molecules. More recent analyses of tetragonal lysozyme crystals simplified the problem even further, and considered only some of the interactions between molecules (Durbin & Feher, 1990; Monaco & Rosenberger, 1993). These analyses suggested that the habits of the crystals and some other experimental observations could be explained by PBC considerations. However, as for inorganic crystals, further information on the growth process could not be inferred.

In theory at least, PBC analyses are capable of predicting the molecular growth mechanisms, surface packing arrangements, and other aspects of the growth of any crystal. The fact that they are used infrequently for this purpose in crystal growth studies is primarily because of two requirements which are not easily accomplished. The first of these is the need to determine all the possible periodic bond chains or connected nets in the crystal structure. The enormous number of possible PBC's in any crystal structure (Bennema, 1993), makes this a tedious process even with the aid of computer algorithms. The second requirement of this theory is that

from this large number of possible PBC's, the dominant ones responsible for the formation of the crystal must be selected. The theory does provide a selection mechanism by assuming that the strongest PBC's in the structure are the dominant ones. However, in order to select the strongest PBC's, all the interaction energies between the molecules in the crystal and those between the molecules and the solvent must be determined. Calculating these energies is not a straightforward matter even for small-molecule crystals (Bennema & van der Eerden, 1987; Bennema, 1993). For proteins the variety of possible interactions, including electrostatic, hydrophobic and van der Waals interactions, complicates the problem even further. As a result, most PBC analyses have resorted to numerous simplifications and are usually employed for the more limited goal of predicting the crystal habits of inorganic crystals. Even here, possibly as a result of the approximations made in determining the interaction energies, such as neglecting solvent effects, PBC analyses have not always predicted the crystal habit correctly (Hartman, 1987).

In a recent study Konnert, D'Antonio & Ward (1994) constructed a more complete molecular model of the (110) face of tetragonal lysozyme without employing PBC considerations. Their approach was geometric and visual, employing an exact shape of the lysozyme molecules along with the correct orientations in a two-dimensional representation. This enabled identification of the possible choices for the (110) face: a plane containing the fourfold screw symmetry axes (the 4_3 axes) or one containing the twofold screw symmetry axes (the 2_1 axes). The molecular images for these two possibilities were then compared with images obtained by atomic force microscopy (AFM) scans on the (110) face of growing crystals. The comparisons indicated that the plane defined by the 2_1 axes was most likely to be the (110) face. The predictions by earlier investigators employing simplified PBC analyses (Durbin & Feher, 1990; Monaco & Rosenberger, 1993), were shown to be incorrect. Clearly, simplified or incomplete PBC analyses may in certain instances lead to erroneous predictions, while the approach of Konnert and coworkers may hold some advantages for protein crystals.

In this study we propose an approach to analyzing the structure of tetragonal lysozyme crystals which combines the method of Konnert *et al.* (1994), with a traditional and more complete PBC analysis. The geometric method of determining the surface structure of Konnert and coworkers was primarily motivated by the need for comparisons with AFM images. However, it has the advantage of representing the details of molecular orientations in the crystal packing arrangements which are absent in traditional PBC representations. As a result, the number of possible PBC's in the crystal can be reduced to those that incorporate the lysozyme molecules with all the molecular orientations found in the crystal structure. A thorough analysis of all the intermolecular contacts in the tetragonal structure will also be undertaken in this study, which should facilitate the unambiguous selection of the dominant PBC's. Finally, wherever possible, the morphology of crystal faces, edges and vertices predicted by this analysis will be compared with images obtained from AFM, electron microscopy and etching studies by other investigators, in order to confirm predictions or resolve available choices in the packing arrangement.

The goals of this study will be more ambitious as well. In addition to predicting the crystal habit, we intend to determine the molecular crystallization mechanisms of the faces of tetragonal lysozyme. Studies employing AFM and other techniques have revealed several interesting morphological features during the growth of these crystals. For example, on the (110) face both growth islands and etch pits were found to be elongated in the [$\bar{1}$10] direction and the growth step height on this face was found to be two molecules high (Durbin & Feher, 1990; Durbin & Carlson, 1992; Durbin, Carlson & Saros, 1993; Monaco & Rosenberger, 1993; Konnert *et al.*, 1994). Studies of the growth kinetics have indicated that the crystallizing units may not be the monomeric protein molecules, but higher order aggregates such as tetramers and octamers (Nadarajah, Forsythe & Pusey, 1995; Li, Nadarajah & Pusey, 1995; Nadarajah, Li & Pusey, 1996). We will attempt to verify and explain these and other observations here.

2. Method of analysis

The crystallographic coordinates of hen egg-white lysozyme in the tetragonal form (shown in Fig. 1), were obtained from the Protein Data Bank (Diamond, 1974). The visualization and analysis of the packing

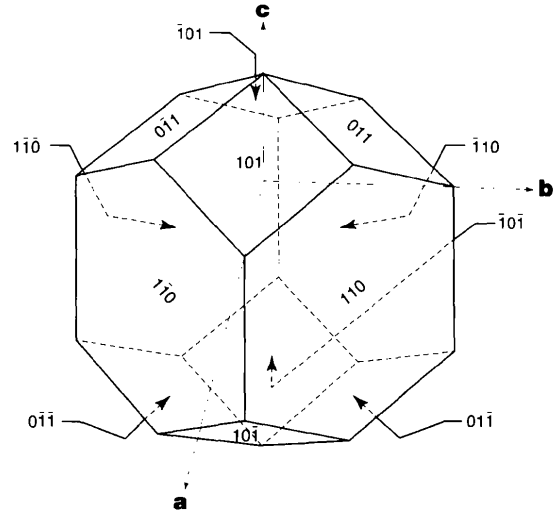

Fig. 1. Illustration of the growth habit of tetragonal lysozyme crystals showing the various faces.

arrangements and the intermolecular bonds were accomplished with the commercial program *QUANTA* (Molecular Simulations Inc., Waltham, Massachusetts), implemented on a Silicon Graphics Iris workstation. The construction of the crystal model involved suitably assembling molecules with the eight unique orientations which make up the unit cell. The reference molecule is labeled *M* and the other seven molecules are labeled *A–G*, with the displacement of each of them with respect to the reference molecule given in Table 1 (*International Tables for Crystallography*, Vol. A, No. 96, 1983).

The unit cell containing these eight molecules is shown in Fig. 2, as viewed along the *c* axis, together with its simplified representation. The simplified representation makes it possible to distinguish the different molecules in the cell while still retaining the molecular orientation information, similar to the representation used by Konnert *et al.* (1994). The space occupied by each lysozyme molecule (the asymmetric unit) is represented by a rectangular block of dimensions 28.0 × 28.0 × 37.9 Å. This is illustrated in Fig. 3 with the sides of the block numbered from 1 to 6. Side 2 faces the active site of lysozyme. Each face of the block represents one or more interactions with nearest neighbors. This representation of the lysozyme asymmetric unit and its dimensions are dictated by

Table 1. *The positions and molecular interactions in the unit cell of tetragonal lysozyme with a space group of* $P4_32_12$

The primed molecules are in the cell immediately below, and the double primed ones in the cell immediately above, the reference unit cell. The interactions shown are only those with the reference molecule *M*. The interatomic bonds that constitute each interaction are separated according to type in Table 2.

Molecule	Position	Interaction label	No. of bonds
M	X, Y, Z	—	—
M′	$X, Y, Z-1$	*V*	1
M″	$X, Y, Z+1$	*V*	1
A	$-X, -Y+1, \frac{1}{2}+Z$	—	0
B	$\frac{1}{2}-Y, \frac{1}{2}+X, \frac{3}{4}+Z$	*Z*	22
B′	$\frac{1}{2}-Y, \frac{1}{2}+X, -\frac{1}{4}+Z$	*W*	10
C	$-\frac{1}{2}+Y, \frac{1}{2}-X, \frac{1}{4}+Z$	*W*	10
C′	$-\frac{1}{2}+Y, \frac{1}{2}-X, -\frac{3}{4}+Z$	*Z*	22
D	$\frac{1}{2}-X, \frac{1}{2}+Y, 1\frac{3}{4}-Z$	—	0
E	$\frac{1}{2}+X, \frac{1}{2}-Y, 1\frac{1}{4}-Z$	—	0
F	$Y, X, 1-Z$	*Y*	33
G	$-Y, -X, 1\frac{1}{2}-Z$	*X*	10

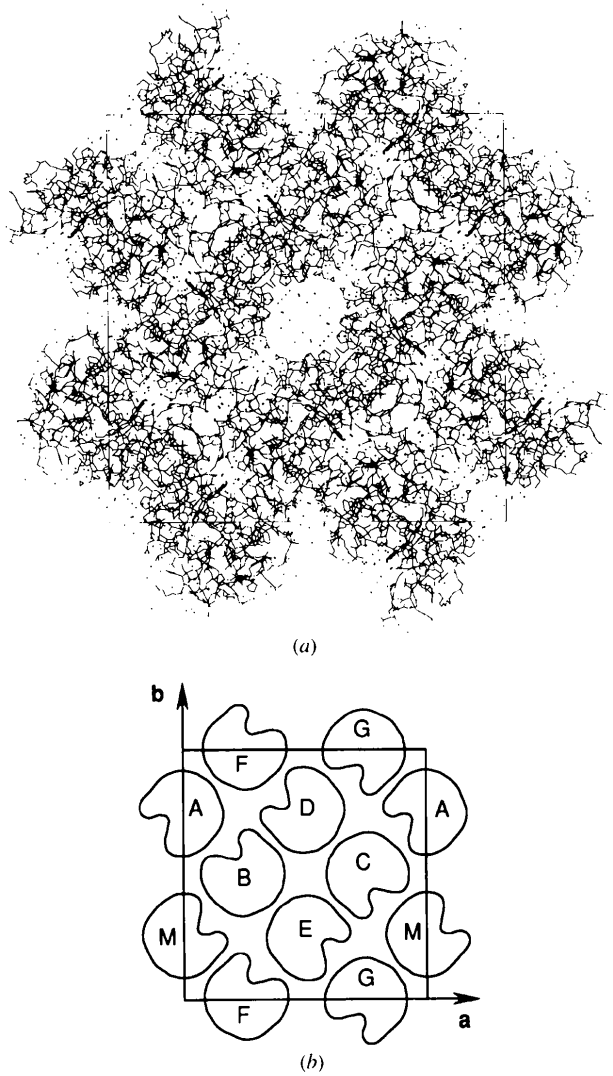

Fig. 2. The unit cell of the tetragonal lysozyme crystal as viewed along the *c* axis, (*a*) in a view of the molecular packing including the bound solvent molecules, and (*b*) in a simplified representation indicating the symmetries in the molecular orientations. The positions of the eight molecules of the unit cell are listed in Table 1.

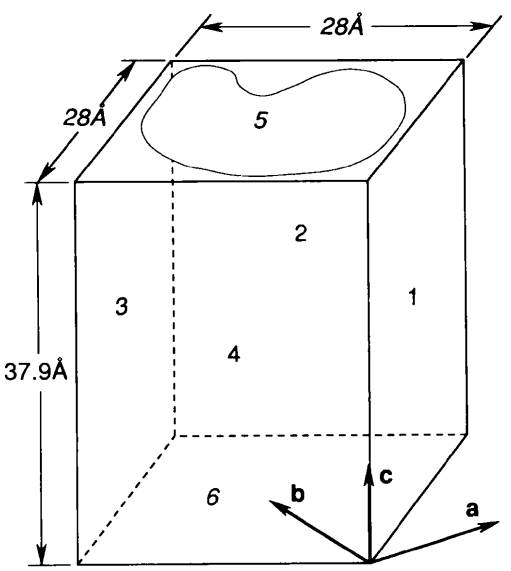

Fig. 3. The rectangular block representation of the lysozyme asymmetric unit in tetragonal crystals. The reference molecule *M* is shown here with the numbering convention for the sides.

Table 2. *The number of different types of interatomic bonds that constitute each interaction*

Note that only one salt bridge is listed for the *X* interaction as the intramolecular salt bridge here is stronger than the intermolecular one.

Interaction	Hydrogen bonds	Water-mediated hydrogen bonds	Salt bridges	van der Waals/ hydrophobic bonds	Total number of bonds
V	0	1	0	0	1
W	2	4	0	4	10
X	2	5	1	2	10
Y	14	12	0	7	33
Z	5	9	1	7	22

the tetragonal space group $P4_32_12$ of the crystal and the 79.1 × 79.1 × 37.9 Å dimensions of the unit cell (Imoto *et al.*, 1972). Other crystal forms may dictate different representations, such as hexagonal blocks for the packing found in the monoclinic rubredoxin crystals (Frey *et al.*, 1988, 1992).

The structures of the reference molecule *M* and the nine other molecules surrounding it were systematically searched to identify all interatomic bonds between them. A cutoff of 4.0 Å was used to determine all hydrogen bonds, salt bridges and van der Waals/hydrophobic bonds. With the exception of a few discrepancies, most of the interatomic contacts agreed with those listed by earlier investigators (Moult *et al.*, 1976). Furthermore, all water-mediated hydrogen bonds between molecules and anion-mediated salt bridges were also determined. The importance of these in stabilizing the interactions between proteins and ligands has been shown recently (Grubmüller, Heymann & Tavan, 1996). The results are given in Table 2. To avoid confusion we will, henceforth, refer to the total force arising from the sum of individual interatomic bonds/contacts between *M* and a neighboring molecule as an interaction as shown in Tables 1 and 2. Thus, the periodic bond chains will actually consist of chains of interactions.

The PBC's present in various slices in the crystal were determined. In traditional PBC analyses of inorganic crystals, complete PBC's which reproduce the stoichiometry of the crystalline material and which do not have breaks in the chain are distinguished from other primitive PBC's (Hartman, 1987). It is these complete PBC's which are considered to be responsible for the growth of the crystal. Protein crystals lack such stoichiometry requirements, but they do have molecular orientation requirements not found in inorganic crystals. We will consider the stoichiometry of protein crystals to consist of the eight unique molecular orientations in the crystal structure, and the complete PBC's to be ones that reproduce these orientations in proportion without breaks in the chain. This requirement narrows the list of possible PBC's in tetragonal lysozyme that need to be considered.

3. Results and discussion

3.1. *Molecular orientations and interactions*

There are eight other molecules interacting with every lysozyme molecule in the tetragonal crystal structure, two for each of the block faces 2 and 3, and one for faces 1, 4, 5 and 6. These are shown in Fig. 4, with the molecular positions listed in Table 1. Molecules *B*, *B'*, *C* and *C'* are related by fourfold screw symmetry to the reference molecule *M*, while *F* and *G* are related by twofold symmetry (*International Tables for Crystallography*, Vol. A, No. 96, 1983). Molecules *B*, *B'*, *C*, *C'* and *G* will be translated relative to *M* along the *c* axis by $+\frac{3}{4}$, $-\frac{1}{4}$, $+\frac{1}{4}$, $-\frac{3}{4}$ and $-\frac{1}{2}$ units, respectively (Fig. 4). Molecule *F* is on the same level as *M*.

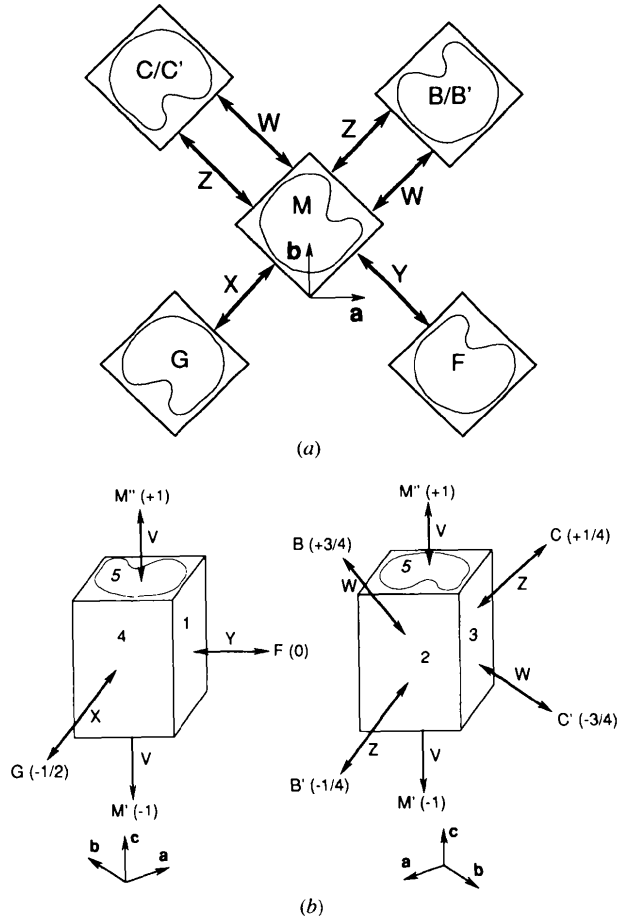

Fig. 4. Illustration of the nearest neighbor interactions for the reference molecule *M*. The view (*a*) along the *c* axis shows six interactions, while the other views (*b*) show all the interactions but with only labels used for the neighboring molecules. The translation of the molecules along the *c* axis with respect to *M* is given in parentheses.

Only five of the eight interactions between *M* and its nearest neighbor molecules are unique and are labeled *V–Z* similar to the convention used in previous studies (Durbin & Feher, 1990; Monaco & Rosenberger, 1993). These are illustrated in Fig. 4 and listed in Tables 1 and 2. Interactions *W* and *Z* are 'head-to-side' interactions between molecules related by fourfold screw symmetry and lead to the formation of a regular helix oriented along the 4_3 axis. The strong *Z* interaction incorporates the effect of an anion located between the *M* and *C* molecules, bridging positively charged groups on both (Blake, Mair *et al.*, 1967; Lim, Nadarajah & Pusey, 1996). [This is the only anion location between molecules in the tetragonal lysozyme structure, the three other locations are all within isolated pockets on each molecule (Lim *et al.*, 1996).] The *Z* interaction connects one molecule to another on the same level, while *W* connects it to one on the next level. Interactions *X* and *Y* connect each helix to neighboring helices. The interaction *Y* is the strongest of the five and is formed by a 'side-to-side' interaction. The *X* interaction is a 'tail-to-tail' interaction incorporating the double intermolecular salt bridge between Lys13 and the C terminus. The weakest is the *V* interaction connecting each molecule to one immediately above and below it along the *c* axis.

It is worth remarking here that estimating the strength of these interactions by merely counting the number of constituent interatomic bonds may underestimate the magnitude of the *W* and *Z* interactions. Although lysozyme has an overall positive charge at the usual growth conditions for tetragonal crystals, with a charge of +11.5 at pH 4.0, the cleft is predominantly negatively charged (Dao-Pin, Liao & Remington, 1989). This facilitates the binding of the largely electropositive and hydrophobic substrates of lysozyme in the cleft region (Blake, Johnson *et al.*, 1967). In this lysozyme resembles the activity of many other enzymes, such as superoxide dismutase (Koppenol, 1981), where the enzyme binds with a substrate of the same overall charge by way of an oppositely charged active site. Studies have shown that the geometry of the active site can act as a focusing device, extending the range of its electrostatic field to the surrounding region, directing the approach of the substrate to the active site (Klapper, Hagstrom, Fine, Sharp & Honig, 1986; Sharp, Fine & Honig, 1987). Clearly a strong bond should result when the negatively charged active-site region of one lysozyme molecule interacts with a predominantly positively charged region of another. These are precisely what the *W* and *Z* interactions represent. The contributions from the long-range electronegative field originating from the cleft, with electropositive groups on the surfaces of the other molecules, are neglected when the interactions are estimated from atomic contacts with a 4 Å cutoff. Thus, the *W* and *Z* interactions may be much larger than that indicated by the list of contacts in Table 2.

Fig. 5 shows the [001] projection of the tetragonal crystal structure. For convenience we will use the thickness d_{hkl} of a slice to designate the slice itself as shown in this figure. In some instances this will correspond to the thickness in the projection, such as for the d_{110} and d_{100} slices, but not for others, such as for the d_{101} and d_{111} slices. An important observation here is that, with the exception of the d_{001} slice, all the others are comprised of double molecular layers in the tetragonal structure.

Fig. 5 also shows that the twofold symmetry axes lie on the (001) plane and run between neighboring 4_3 helices. Although not shown here, there are also twofold symmetry axes on this plane which bisect the helices (*International Tables for Crystallography*, Vol. A, No. 96, 1983). This implies that molecules will be oriented in opposite ways along the *c* axis in neighboring helices, *e.g.* the helices formed by *M–C–A–B–* and by *F–E–G–D–* in Fig. 5. The axes in the [001] direction

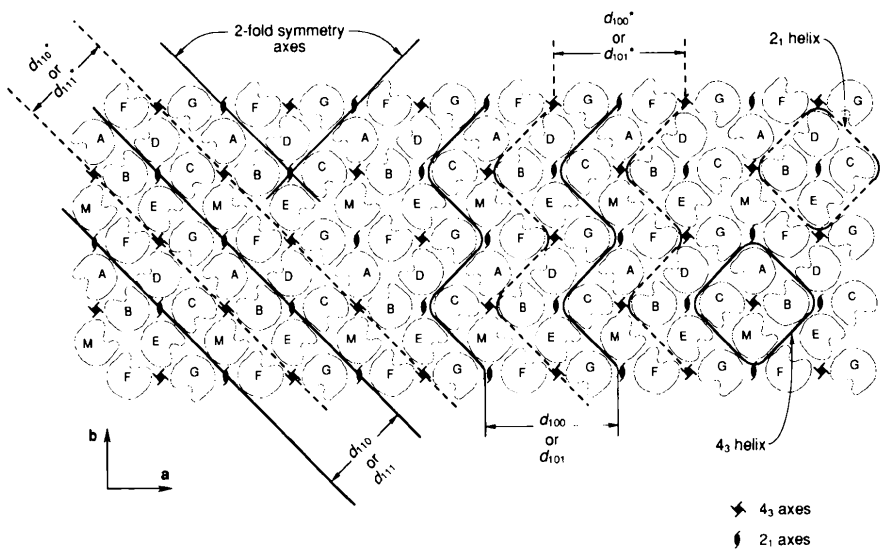

Fig. 5. Packing arrangement in tetragonal lysozyme crystals as viewed along the *c* axis (the [001] projection). The view shown here is an extension of the representation in Fig. 2(*b*) to several unit cells, and shows the three symmetry axes of the $P4_32_12$ space group. The two possible helices in the structure are shown along with the two sets of the d_{110}, d_{101}, d_{111} and d_{100} slices corresponding to these helices. Note that in this figure d_{101} and d_{111} refer only to those slices in this plane and not their true thickness. The slices corresponding to the 2_1 helix are drawn with dashed lines and identified with an asterisk.

along which any four helices meet define the twofold screw symmetry axes (the 2_1 axes) of the structure. It should be noted here that the four molecule helical unit *M–C–A–B* is a repeating arrangement in the entire crystal. In other words, this can be considered as a basic building block for constructing the long-range order in the crystal. This will be an important consideration in the following sections.

3.2. *Periodic bond chain analysis*

From Fig. 5 it can be seen that there are several primitive periodic bond chains or connected nets running through the crystal structure. For example, in the d_{110} slice there are two PBC's in the direction comprising the molecular sequences *M–C–D–F–M–* and *A–G–E–F–A–*. Although these PBC's can be constructed without breaks in the chain, neither of them will reproduce all the molecular orientations of this slice individually. Both are required to construct the slice which implies that both of them together will form a complete PBC. Similarly, two primitive PBC's made up of the molecular sequences *M–C–A–F–M–* and *B–D–G–E–B–* are required for the complete [010] PBC in the d_{101} slice. Thus, the molecular orientation requirement determines that all complete PBC's in the crystal structure will consist of bimolecular layers. This is a consequence of almost all slices in the structure consisting of bimolecular layers.

The molecular orientation requirement by itself may not be adequate to define the complete PBC's that control the crystal growth process. In inorganic crystals the stoichiometry requirement of complete PBC's was formulated to satisfy the electroneutrality condition. As individual protein molecules will satisfy this condition it does not impose any restrictions for protein crystals. However, tetragonal lysozyme crystals have another powerful reason requiring that all the complete PBC's be double layered. By far the dominant PBC in the structure is the one formed by the 4_3 helix. This is a tightly packed and strongly bonded helix, constructed by six bonds (two *V*, two *W* and two *Z* bonds) linking each molecule to others in it. As we will discuss later, it is the PBC formed by this helix that is responsible for many features of the molecular growth mechanism of the crystal. The role of the other PBC's are, thus, relegated to connecting the different 4_3 helices to each other. Given the bimolecular thickness of this helix, the PBC that forms each helix and those that connect them to each other are all necessarily double-layered PBC's.

With these considerations, when the crystal structure was searched for complete PBC's only three were found and these are listed in Table 3. Two of these will be along the [001] projection plane shown in Fig. 5 and will be in the [$\bar{1}$10], [010] and their symmetry-related directions. These PBC's are the weaker ones connecting the strongly bonded 4_3 helices with each other. The [010] PBC is an 'undulating' chain, while the [$\bar{1}$10] PBC is a straight chain (Hartman, 1987). The third PBC will

Table 3. *The complete PBC's in tetragonal lysozyme crystals*

For the [$\bar{1}$10] and [010] PBC's only the interactions involved between the 4_3 helices are listed (see text).

Complete PBC	Type	Bonds involved
[001]	Straight chain	*V*, *W*, *Z*
[$\bar{1}$10]	Straight chain	*X*, *Y*
[010]	Undulating chain	*X*, *Y*

be in the [001] direction perpendicular to this plane, comprises the bonds forming the 4_3 helices, and as mentioned earlier is the strongest of the three. These three PBC's will only form a correspondingly limited number of slices, namely the d_{110}, d_{101}, d_{111}, d_{100}, d_{001}, d_{221} and their symmetry-related slices.

3.3. *Selecting the dominant helix*

We have already discussed how the bimolecular layer slices in the tetragonal structure lead to PBC's that are also necessarily bimolecular. Another consequence is that it gives rise to two possible ways of describing the slices themselves. Correspondingly, there are two possible ways that the basic three PBC set can be constructed as well. The second or alternate set of slices are shown in broken lines and identified with * symbols in Fig. 5. Thus, the correct set of slices must first be identified before proceeding with the analysis of the slices.

The two sets of slices arise from the two ways the basic helix can be constructed in the tetragonal structure. These two helices are illustrated in Fig. 6. The first of these is the helix described in the previous sections and is formed by the molecular sequences *M–C–A–B–M″–* . . . or *F–E–D–G–F″–* . . . in Fig. 5,

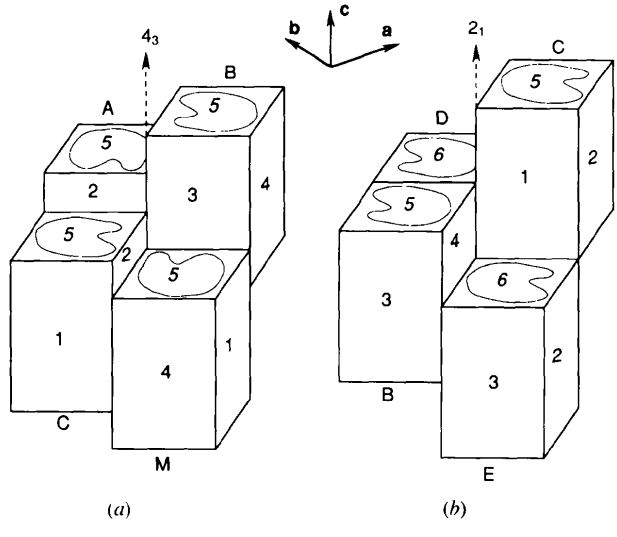

(*a*) (*b*)

Fig. 6. The four-molecule helical unit of (*a*) the regular 4_3 helix and (*b*) the irregular 2_1 helix. The lateral dimensions of both units are 56 Å (see Fig. 3).

centered around the 4_3 axes. It is referred to here as the regular helix as each molecule translates $\frac{1}{4}$ unit along the c axis from the previous one and interacts with the same set of W and Z bonds with the previous and the following molecules in the sequence (Figs. 4 and 6*a*). The second or alternate helix is constructed about the 2_1 axis by the molecular sequences *M–F–A–G–M′′–* . . . or *D–C–E–B–D′′–* . . . in Fig. 5. Strictly speaking this arrangement is not a helix as only every other molecule in the sequence is translated by $\frac{1}{2}$ unit from the previous molecule along the c axis. For the sake of argument we will refer to it here as the irregular helix. The bonds between molecules in its sequence alternate between the stronger Y bond and the weaker X bond (Figs. 4 and 6*b*). The alternate set of slices correspond to this irregular helix and there will be an alternate set of three complete PBC's corresponding to it as well.

It should be clear from Tables 1 and 2 that the regular 4_3 helices are far stronger than the irregular 2_1 helices. Each molecule in the 4_3 helix is bonded to others in it by two W and two Z interactions (we have neglected the weak V interactions). These represent a total of 64 interatomic bonds. On the other hand, each molecule in the 2_1 helix is bonded by one X and one Y interaction, representing a total of only 43 interatomic bonds. As mentioned earlier, the W and Z interactions may be even larger than that indicated by the number of contacts due to long-range electrostatic fields originating in the active sites of lysozyme molecules. Finally, each helix can be regarded as being only as strong as its weakest link. In the case of the irregular 2_1 helix this is the weak X interaction representing merely ten interatomic bonds. The regular 4_3 helix, however, does not have a weak link as each molecule is linked in exactly the same way: by two Z interactions to molecules before and after it on the same level and by two W interactions to molecules in the levels above and below it (Figs. 4 and 6*a*).

If the 4_3 helix is the dominant one as predicted above, then the slices and PBC's associated with it control the crystal growth process, and the molecular packing arrangements on the crystal faces can be determined. For example, the (110) face will be formed by the plane containing the 2_1 axes in the $[\bar{1}10]$ or [110] directions, *i.e.* it is formed by the d_{110} slice. This has been demonstrated by high resolution AFM scans on the (110) faces of tetragonal lysozyme by Konnert *et al.* (1994). It was clearly shown that the (110) faces are formed by the PBC's associated with the 4_3 helices. This agreement between predictions from PBC considerations and AFM scans will serve as the basis for constructing the surface morphology and the growth mechanisms of the crystal faces in the following sections.

Although this result seems clear enough, the previous two investigations of tetragonal lysozyme concluded that the PBC's corresponding to the irregular 2_1 helix were the controlling ones in the crystal growth process (Durbin & Feher, 1990; Monaco & Rosenberger, 1993).

Table 4. *The list of six possible planes giving the thickness of the slices, the PBC's that form them and the resulting face types on the crystal*

Slice	Thickness (Å)	PBC's	Face type
(110)	55.9	$[\bar{1}10]$, [001]	*F*
(001)	37.9	$[\bar{1}10]$, $[1\bar{1}0]$	*F*
(100)	79.1	[001], [010]	*F*
(101)	34.2	[010]	*S*
(111)	62.8	$[\bar{1}10]$	*S*
(221)	35.9	$[\bar{1}10]$	*S*

However, it is easily seen that this was based on the simplifications adopted by those studies. The V and W interactions were neglected and the X and Y interactions were considered to be larger than the remaining two Z interactions. This error arose because the interatomic contacts were not individually determined as done here, but was based on the number of adjacent residues between neighboring molecules listed by earlier investigators (Moult *et al.*, 1976). They also failed to notice the irregularity of the 2_1 helices and that they were no stronger than the weakest link, namely the X interaction.

3.4. *Morphology and growth mechanism of the (110) face*

The determination that the dominant PBC's in tetragonal lysozyme are those listed in Table 3, as discussed in the previous section, allows morphology of the crystal faces to be determined. Table 4 shows that the d_{110} slice contains two PBC's: the $[\bar{1}10]$ chain and the [001] chain. As mentioned before, the [001] chain is the strongest one involving the formation of the 4_3 helices. The weaker $[\bar{1}10]$ chain, and its symmetry-related [110] chain, connect the helices to each other and also bind the d_{110} slices to each other. The presence of two straight chain PBC's on this slice indicates that this is a planar F face.

Table 4 shows that there are two other possible F faces, the (001) and the (100), neither of which is seen on the crystal. Of these it is easy to see why the (001) is not formed as the PBC's along the d_{001} slice are weak while the strong [001] PBC is perpendicular to it. Attachment is more likely to occur in the [001] direction preventing the formation of the (001) face. The reason for the absence of the (100) face is less clear. Both the d_{110} and the d_{100} slices share the [001] PBC (Fig. 5). The other PBC's, the $[\bar{1}10]$ chain for the d_{110} and the 'undulating' [010] chain for the d_{100}, are of comparable strength. However, the undulating nature of the [010] chain will make the (001) a rough face, usually harder to form. This could result in the preferential formation of the smoother (110) face on the sides of the crystal.

The d_{110} slice has two molecular layers and the growth of the (110) face will involve the first layer being formed by the X and Y interactions. The next layer will be formed by the stronger double W and Z interactions (two W and two Z interactions for each

X and Y interaction combination). Thus, the formation of the first layer should be the rate-limiting step, with the second layer formed immediately upon deposition of the first. This suggests that both layers, or at least the smallest component of both layers, is deposited on the surface simultaneously. This smallest component is the four-molecule helical combination illustrated in Fig. 6(*a*). The above considerations imply that this is a crystallizing unit for the (110) face.

Further evidence for the four-molecule crystallizing unit comes from microscopic studies of the (110) face which showed that the growth layers on this face were always composed of double layers (Durbin & Feher, 1990; Durbin & Carlson, 1992; Durbin *et al.*, 1993; Konnert *et al.*, 1994). The ~56 Å height of the double layer, corresponding to the dimensions of this tetramer unit (Figs. 3 and 6*a*), has also been confirmed by AFM measurements (Konnert *et al.*, 1994). If the two layers are formed sequentially, incomplete monolayers would have been seen in these studies. The absence of monolayers on the (110) face, thus, implies the simultaneous formation of the double layer with the tetramer the smallest crystallizing unit for this process. Clearly, the entire (110) face can be constructed with this unit, because this is a building block for the entire tetragonal lattice structure as discussed earlier (Fig. 5).

Strictly speaking, the smallest crystallizing unit for the formation of the double layer is a dimer. However, such a dimer will have unsatisfied Z and W interactions. The arguments used to suggest the simultaneous attachment of two molecules will also require that the tetramer be formed simultaneously in order to complete these bonds in one helical layer. Fig. 7 illustrates this process. The rate-limiting step is the attachment of the first molecule on the crystal face by the weaker X and Y interaction combination. This is followed by the rapid completion of the helical unit by the addition of three other molecules with identical strong W and Z interaction combinations, indicating the nucleation of the tetramer crystallizing unit. There will be too many exposed W and Z interactions if the unit is any smaller than a tetramer, making this the minimum size for a crystallizing unit on this face.

In the formation of the crystallizing unit, further attachment beyond the minimum number by rapid reactions cannot occur in the [$\bar{1}$10] direction as more molecules can only be added with the weaker X and Y interaction combination. However, as the helix and the strong PBC associated with it continue in the [001] direction, it introduces the possibility that the crystallizing unit may be even larger, such as an octamer. As shown in Fig. 7, following the attachment of the first molecule, all other attachments along the helix proceed without a break by the same strong W and Z interaction combination.

The observation that growth islands and etch pits on the (110) face are both elongated in the [$\bar{1}$10] direction suggests that the crystallizing unit may be an octamer (Durbin & Feher, 1990; Monaco & Rosenberger, 1993). The preferential dissolution in the [$\bar{1}$10] direction during etching may be explained by the weaker PBC in that direction, but this argument will predict that the growth

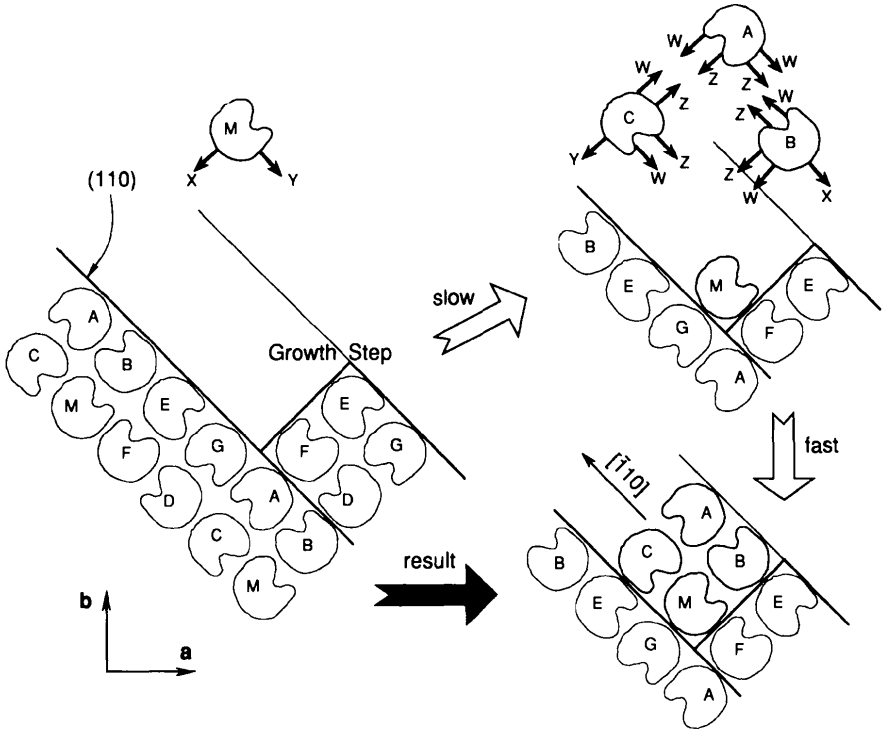

Fig. 7. Illustration of the spontaneous nucleation of a tetramer crystallizing unit on a growth step on the (110) face. The initial slow attachment of a molecule by an X and Y interaction combination is followed by the rapid attachment of three molecules by W and Z interaction combinations, completing the helical tetramer. The net result is the nucleation of the tetramer unit.

islands should then be elongated in the [001] direction instead. An octamer crystallizing unit resolves nicely this contradiction as shown in Fig. 8. The preferred attachment direction for such a unit is [$\bar{1}$10] as this will maximize the contact region for the unit. Additionally, unlike between tetramer units in the [$\bar{1}$10] direction, between octamer units in this direction there are two [$\bar{1}$10] PBC's which exceeds the strong, but single, [001] PBC. Similarly the preferred dissolution direction is also [$\bar{1}$10] as the units comprising the pit walls are less securely attached in this direction. As shown in Fig. 8 the dissolution in the [001] direction will require the detachment of octamer units completely enclosed on three sides.

The reason for growth and dissolution by octamer units is not immediately obvious. As discussed earlier the PBC structure requires that the crystallizing unit be at least a tetramer. Why should the growth unit be an octamer and not a larger or smaller unit? A possible reason may be that a tetramer unit on the (110) face will still have unsatisfied bonds in the [001] direction, facilitating the formation of still larger units in this direction. However, it will be increasingly difficult to form large units on the growth face spontaneously. Thus, octamer units may represent a compromise between these two tendencies, enabling the (110) face to be formed by this unit.

3.5. *Morphology and growth mechanism of the (101) face*

Table 4 shows that the d_{101} slice has only one PBC running through it. This is illustrated in Fig. 9, which shows the projections in the [010] and [001] directions.

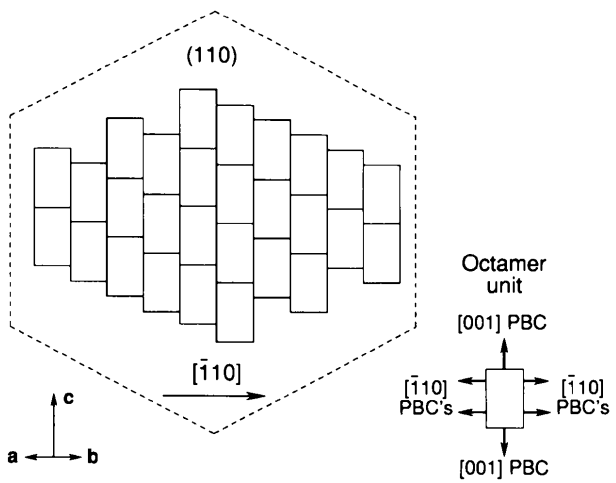

Fig. 8. Illustration of the growth/dissolution anisotropy on the (110) face with octamer crystallizing units. Growth is facilitated in the [$\bar{1}$10] direction over [001] as at least two PBC's are formed in this direction during attachment, against one in the [001] direction. Dissolution in the [001] direction requires removal of a unit enclosed on three sides, while removal of a unit in the [$\bar{1}$10] direction is easier to accomplish.

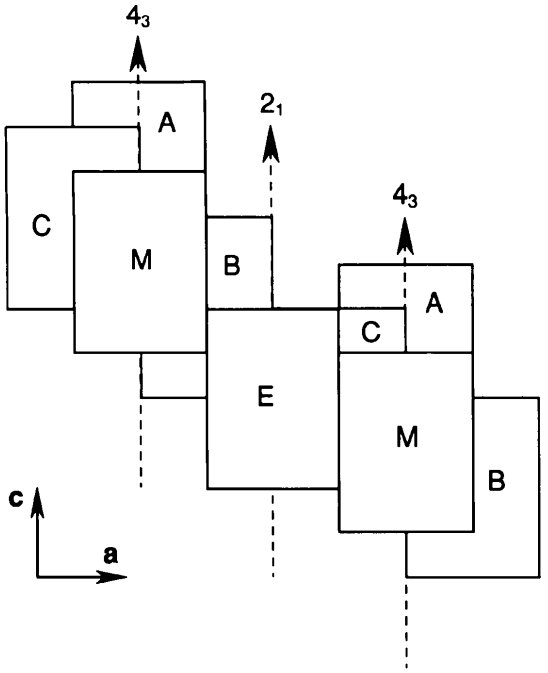

(*a*)

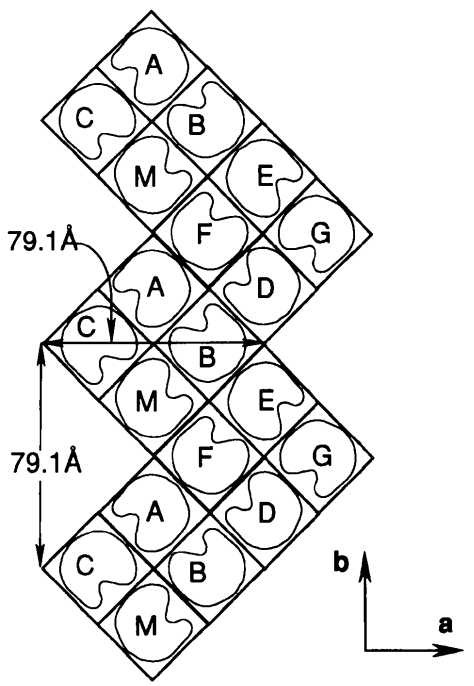

(*b*)

Fig. 9. The d_{101} slice: (*a*) the [010] projection, where the thickness of the slice is 34.2 Å, showing the absence of any complete PBC's along the plane of this projection, and (*b*) the [001] projection, showing the [010] PBC and that the distances between edges in the *a* and *b* directions correspond to the unit-cell dimensions in those directions as seen experimentally (Durbin & Feher, 1990).

The helical units are shown about the 4_3 axes. Along the 2_1 axes where the helices meet there are no interactions between the tetramer units along the (101) plane. Fig. 9(*a*) shows that there is no complete PBC along the [010] projection, although a primitive PBC through molecule *E* exists. The only complete PBC is the undulating [010] chain seen in Fig. 9(*b*). Thus, (101) is essentially an *S* face.

Table 3 also shows that there are two other possible *S* faces: the (111) and the related (221). Both of these are formed by the $[\bar{1}10]$ PBC, which is comparable to the [010] PBC forming the (101) face. However, only the (101) faces are visible in the grown crystal. In the previous section it was suggested that for the *F* faces, the [010] PBC may be harder to form than the $[\bar{1}10]$ PBC because of its undulating nature, despite their comparable strengths. It is not very clear why the (101) face is preferred over the (111) and (221) faces. A possible reason may be the partial roughness of *S* faces, which makes them relatively rare occurrences as crystal faces (Hartman, 1987). The *S* faces that do form are likely to be the ones with the weakest PBC's. This probably causes the appearance of (101) faces on tetragonal crystals instead of the (111) and (221) faces. However, these latter faces do form when the crystals are etched (Monaco & Rosenberger, 1993), indicating that the energy levels for the three faces are not too different.

The same arguments employed to suggest that the crystallizing unit for the (110) face must at least be a tetramer are equally valid for the (101) face as well. Microscopic studies of the (101) face have shown that it grows by the formation of monolayers, unlike the (110) face (Durbin & Feher, 1990; Durbin & Carlson, 1992; Durbin *et al.*, 1993). This corresponds to the 34.2 Å thickness of a single d_{101} slice shown in Fig. 9(*a*). Note that growth by a $\frac{1}{2}$ d_{101} slice does not imply growth by monomer crystallizing units, as this would correspond to a layer of d_{101} thickness, which has not been observed. This also precludes the growth of this face by crystallizing units which are larger in the [001] direction, such as the octamer units on the (110) face. Thus, the experimental evidence suggests that the crystallizing unit for the (101) face is a tetramer. Other evidence for this growth mechanism and surface morphology is provided by the undulating or jagged edge of this face as shown in Fig. 9(*b*). The high relief of this face allowed Durbin & Feher (1990) to measure the edge-to-edge distances on it, unlike on the low relief (110) face. They found that the distances corresponded to the lattice dimensions in the *a* and *b* directions. Fig. 9(*b*) shows that these are indeed the expected edge-to-edge dimensions of this slice when constructed with tetramer units linked by the [010] PBC.

The most likely reason for the growth unit being only a tetramer, and not a larger one, is the orientation of the crystallizing unit with respect to the (101) face. From Fig. 9 it should be clear that the attachment of an octamer unit to the face will leave half the unit exposed without any interactions, which makes the attachment an unlikely event. In other words, on the (110) face, changing from a tetramer to an octamer crystallizing unit increases its size only in a direction parallel to the face, increasing the area of attachment. On the (101) face, however, such a change will increase the size of the unit in the direction perpendicular to the face as well. This fact should make growth by octamers on the (101) face possible only under unusual conditions such as on a screw dislocation hillock with a Burger's vector with a magnitude twice the repeat distance. Under normal growth conditions attachment of tetramers are to be expected giving rise to monolayer growth, as was observed experimentally (Durbin & Feher, 1990; Durbin & Carlson, 1992; Durbin *et al.*, 1993).

3.6. *Molecular packing on edges and vertices*

An important observation obtained from computer visualization of the packing arrangement in the crystal is the relative roughness of the {110} and the {101} faces. The greater smoothness of the (110) faces can be seen from the perfect alignment of the molecules on the d_{110} slice in Fig. 5. The roughness of the (101) face is easily seen from the views of the d_{101} slice in Figs. 5 and 9. This has been observed experimentally as well. Because of the smoothness of the (110) face the lattice parameters could not be observed on the face by electron microscopy (Durbin & Feher, 1990), and was barely discernible with AFM (Konnert *et al.*, 1994). However, the roughness of the (101) face allowed the lattice parameters to be determined even by electron microscopy (Durbin & Feher, 1990).

The greater roughness of the (101) face is also indicated by the faster growth rates of this face

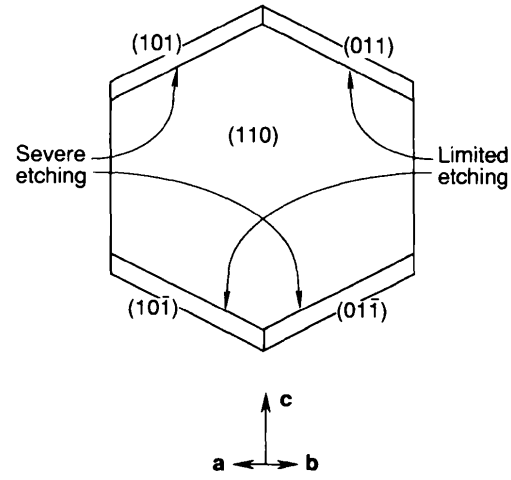

Fig. 10. Illustration of the (110) face of the crystal showing the asymmetric etching pattern observed on the edges with the {101} faces (Monaco & Rosenberger, 1993).

at lower supersaturations, when compared with the smoother (110) face (Durbin & Feher, 1986; Monaco & Rosenberger, 1993; Forsythe & Pusey, 1994). Perhaps more significantly, the smoothness of the (110) face is indicated by its slower dissolution rates during etching of the crystal (Monaco & Rosenberger, 1993). The (110) face remains macroscopically planar throughout the period where the (101) face was being slowly etched, including the relatively rough apex of the crystal where the etching was most pronounced. Etch pits appeared on the (110) face only after prolonged etching.

The severe etching of the crystals revealed an interesting asymmetry on the edges formed by the (110) and (101) faces as illustrated in Fig. 10 (Monaco & Rosenberger, 1993). The upper left and the lower right edges around the (110) face were etched severely, while the upper right and lower left edges etched less. Monaco & Rosenberger (1993) suggested that the difference in bond structures on these two sets of edges, arising from the fourfold screw symmetry of the crystal, was responsible for this asymmetry. Our analysis, while confirming the differences in bond structures, also indicates a possible reason why this difference should gives rise to the observed etching pattern. Fig. 11 illustrates the molecular arrangement on two adjoining edges. This clearly shows that the edge between the (101) and (1$\bar{1}$0) faces has a relatively smooth molecular arrangement, which cannot be duplicated on the edge between the (101) and (110) faces. The smoother edge is likely to etch more slowly than the rougher one, resulting in the asymmetry.

The other interesting observation on the etching of these edges are the (111) and (2$\bar{2}$1) faces formed

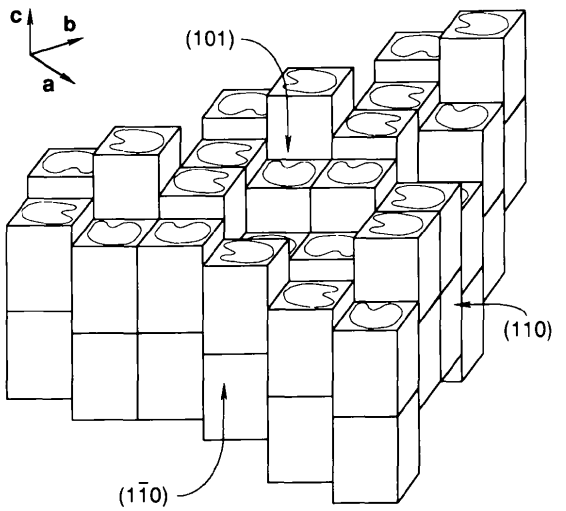

Fig. 11. Rectangular block representation of the edges between the (101) face and the (1$\bar{1}$0) and (110) faces, indicating the asymmetry caused by the fourfold screw symmetry of the crystal. The edge formed by the (1$\bar{1}$0) face is smoother than that formed by the (110) face.

(Monaco & Rosenberger, 1993). From the arguments given in the previous sections, it is easy to see that the natural crystallizing unit is the tetramer for the (111) and the octamer for the (2$\bar{2}$1) faces. During etching the (111) faces formed on the (101) side of the edge, while the (2$\bar{2}$1) faces formed on the (110) side. Thus, even at the edges the dissolution seems to proceed by tetramers on the (101) face and octamers on the (110) face, resulting in the two new faces being formed there in an alternating fashion. This suggests that growth on these edges also proceeds by the crystallizing units of the adjoining faces.

3.7. *Formation of the crystallizing units*

As discussed in the previous sections, both PBC considerations and experimental evidence suggest that tetramer and octamer crystallizing units are responsible for the formation of the (101) and the (110) faces. However, the growth of these crystal faces was assumed to proceed by the spontaneous nucleation of these units on the faces. An alternate growth mechanism is by the formation of these units in the bulk solution, followed by their transport to and attachment on the crystal faces. In this section these two growth mechanisms will be evaluated.

In inorganic systems the formation of non-monomer crystallizing units is dictated by the requirement of electroneutrality, *i.e.* anions and cations are nucleated as stoichiometric crystallizing units on the crystal surface. This driving force will not exist for protein molecules as they will satisfy the electroneutrality condition either individually or by binding counterions. This does not mean that electrostatic attraction between proteins is absent, but that it is much weaker than that between small anions and cations, relative to their size. Additionally, unlike the small ions, proteins have non-uniform charge distributions and irregular geometries which require that they be appropriately oriented for correct bond formation. Such factors contribute to aggregation between the large protein molecules being a complex process, involving the correct orientation of the molecules by electrostatic and hydrodynamic forces (Klapper *et al.*, 1986; Sharp *et al.*, 1987; Luty *et al.*, 1993; Brune & Kim, 1994), and bond formation by electrostatic and hydrophobic forces (Honig, Sharp & Yang, 1993).

These considerations make the spontaneous nucleation of large aggregate units on the crystal surface a very unlikely event. Even for small spherically symmetric molecules, bimolecular reactions are the norm with trimolecular reactions being extremely rare and higher order reactions unknown. For the protein crystallizing units discussed here, it is far more likely that the units are formed sequentially from bimolecular reactions in the bulk solution, by the formation of dimers from monomers, tetramers from dimers and so on. Thus, the nature of the aggregation process suggests that the growth of tetragonal lysozyme crystals proceeds by the

formation of the crystallizing units in solution prior to their attachment on the crystal surface. In other words, the sequence of events depicted in Fig. 7 should be reversed. The tetramers and octamers are first formed rapidly in the bulk solution by the strong W and Z interactions, followed by the slow attachment of the units to the crystal faces by the weaker X and Y interactions.

Evidence that this is indeed the case is provided by studies of lysozyme aggregation and crystal growth kinetics. The presence of lysozyme aggregates in solution have been shown by several investigators employing a variety of experimental methods (Sophianopoulos & Van Holde, 1964; Sophianopoulos, 1969; Zehavi & Lustig, 1971; Studebaker, Sykes & Wien, 1971; Banerjee, Pogolotti & Rupley, 1975; Hampe, Tondo & Hasson-Voloch, 1982; Pusey, 1991; Wilson & Pusey, 1992). The aggregates are formed even in undersaturated solutions and the extent of aggregation increases with supersaturation. Under crystal growth conditions in supersaturated solutions, the higher order aggregates predominate (Boué, Lefaucheux, Robert & Rosenman, 1993; Behlke & Knespel, 1996). The necessary crystallizing units, therefore, already exist in bulk solution under growth conditions.

Further evidence for this mechanism comes from studies of the growth kinetics of the (110) face. These have shown that the growth rate is not a simple function of the supersaturation (Monaco & Rosenberger, 1993; Nadarajah *et al.*, 1995, 1996; Li *et al.*, 1995). The growth rates go to zero asymptotically as the saturation limit is approached, while at high supersaturations the growth rates begin to decrease after reaching a maximum. This unusual growth behavior can be understood if lysozyme in solution is assumed to have an aggregate distribution composed of units from monomers to octamers and higher orders (Nadarajah *et al.*, 1995). As the supersaturation is increased the distribution is altered towards the higher order aggregates. Thus, the concentration of octamers will increase from being asymptotically zero near the saturation limit, reach a maximum and then decrease as still higher order aggregates are preferentially formed. This correspondence between the octamer concentration and the growth rate dependence of the (110) face on supersaturation was confirmed by predictions from a mathematical model of lysozyme aggregation in solution, followed by dislocation or two-dimensional nucleation growth with octamer units (Li *et al.*, 1995; Nadarajah *et al.*, 1996). Comparisons between the model predictions and the measured growth rates showed good agreement, indicating the validity of this mechanism.

Although such extensive investigations have not yet been carried out for the (101) face, the experimental evidence shows that the growth rates on this face also have a similar dependence on the supersaturation (Monaco & Rosenberger, 1993; Forsythe & Pusey, 1994). Furthermore, the (101) growth rates are higher than the (110) growth rates at lower supersaturation. They also reach their growth maximum earlier after which their growth rates decrease to levels below that of the (110) face. These trends are indicative of the growth of the (101) face by an aggregate in solution, but one smaller than the octamers responsible for the growth of (110) faces. A tetramer crystallizing unit would explain these trends. These strongly suggest that tetragonal lysozyme crystals grow by the formation of tetramer and octamer crystallizing units in the bulk solution followed by their transport to and attachment on the {101} and {110} faces. Such a mechanism would also explain the need for high supersaturations for lysozyme crystal growth, as the higher order aggregates are only formed at these supersaturations.

The aggregation studies also provide evidence that these aggregates correspond to the regular 4_3 helix, and not the irregular 2_1 helix. If aggregates formed in the bulk solution correspond to the 2_1 helix, then the activity of the enzyme will not be affected by the aggregation process, because the active site will not be blocked. In the 4_3 helix, however, the active site is blocked as shown in Fig. 12. This figure also indicates that in dimers corresponding to this helix, one of two active sites is blocked. Consequently, even in undersaturated solutions, increasing the concentration of lysozyme should increase aggregate formation leading to decreases in its enzymatic activity. Experimental measurements have shown that the activity does indeed decrease with the concentration (Wilcox & Daniel, 1954; Hampe *et al.*, 1982). Other studies of the aggregation process have further indicated that the dimers formed are not the 'tail-to-tail' or 'side-to-side' dimers (*i.e.* the 2_1 helix dimers), but are either the 'head-to-tail' or the 'head-to-side' dimers (*i.e.* the 4_3

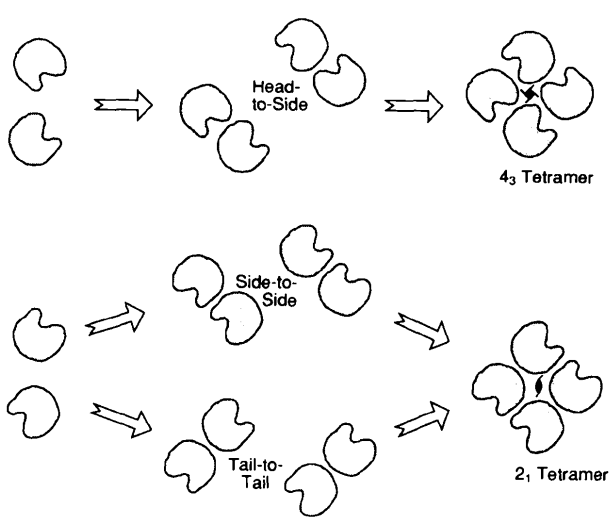

Fig. 12. Illustration of the various types of lysozyme dimers that can be formed during aggregation and the pathways for the formation of the 4_3 and the 2_1 tetramers. Formation of the 4_3 tetramer causes the progressive blocking of the active sites of individual molecules, but not the formation of the 2_1 tetramer.

helix dimers) (Sophianopoulos, 1969; Zehavi & Lustig, 1971; Studebaker *et al.*, 1971; Banerjee *et al.*, 1975). These studies suggest that the aggregates formed in solution have a geometry corresponding to the 4_3 helix (Fig. 12).

4. Concluding remarks

The PBC analysis described here reveals the need to evaluate precisely the relative magnitude of the molecular interaction energies in the protein crystal structure. The evaluation of these relative energies solely from the number of adjacent residues between neighboring molecules can lead to errors. This in turn can result in incorrect predictions of surface morphologies and growth mechanisms. Until recently a method for the precise evaluation of the total interaction energies between protein molecules was not available. However, the investigations of Honig and co-workers (Sharp & Honig, 1990; Honig *et al.*, 1993; Honig & Nichols, 1995) have now made such evaluations, though still a complex task, at least one that can be carried out.

In this study the relative strengths of the five different interactions between molecules in tetragonal lysozyme crystals were estimated from the number of interatomic bonds, including water-mediated hydrogen bonds and anion-mediated salt bridges. These were determined from a systematic search of the crystallographic structures of neighboring molecules, which indicated that the two *W* and two *Z* interaction set were much larger than the *X* and *Y* interaction set. This estimate was confirmed by comparisons of the results from the subsequent PBC analysis with experimental observations. However, the precise evaluation of the bond strengths is still essential to show this conclusively.

The usual definition of a complete PBC (Hartman, 1987), had to be modified for protein crystals and here a definition based on molecular orientations and the dominant helical PBC was employed. This condition resulted in only three double-layered, complete PBC's being found in the tetragonal structure, producing mainly double molecular-layered slices. A related result is that one set of interactions will be larger than another, determining that the tetramer corresponding to the 4_3 helix, rather than one corresponding to the 2_1 helix, becomes the basic building block for the entire crystal, with an associated set of complete periodic bond chains. This tetramer then acts as the crystallizing unit for the rough (101) face, while an octamer comprised of two of these tetramers is the crystallizing unit for the smooth (110) face. Thus, this tetramer, and the [001] PBC that forms it, play a central role in determining the growth mechanism of the crystal. The preference for aggregate crystallizing units over monomers seems to be dictated by the weaker *X*, *Y* interactions between the helices, when compared with those within the helix. This introduces a rate-limiting step in the attachment process as illustrated by the following equation,

$$\text{monomer} \xrightarrow[\text{interactions}]{W \,\&\, Z} \text{crystallizing unit} \xrightarrow[\text{interactions}]{X \,\&\, Y} \text{crystal}.$$

The rate-limiting second step in the above equation causes the formation and accumulation of the crystallizing units in solution by the first step. Formation of the large crystallizing unit then ensures that an adequate number of the weaker *X*, *Y* interaction sets are available for the second step of secure attachment to the crystal face to occur.

Protein molecules lack the simple shapes of small-molecule ions and protein crystals lack the strong ionic bonds formed in small-molecule crystals. Proteins have large irregular geometries and most of them lack a simple dipolar charge distribution or even an amphiphilic character. These considerations along with the requirement of precise molecular orientation in the crystallographic form, ensures that aggregate formation and attachment of molecules or crystallizing units to the crystal face are very slow processes. Thus, unlike for small molecules, the spontaneous nucleation of large crystallizing units cannot occur rapidly, and the formation of such a unit at a specific location on the crystal face must be regarded as a very rare event. Formation of these units, by sequential aggregation, is more likely to occur randomly in the bulk solution from molecular collisions. Lysozyme crystal growth requires the transport of these units formed in the bulk solution to the crystal face and subsequent attachment there. This is an essential difference between the commonly observed growth mechanisms of inorganic, small-molecule crystals and that of tetragonal lysozyme. It may be the principal reason for the observed deviations of lysozyme crystal growth from expected behavior.

This work was supported by grant NAG8-984 from the NASA/Marshall Space Flight Center. It is a pleasure to acknowledge discussions with colleagues in the Netherlands: Professor Piet Bennema of the Laboratory of Solid State Chemistry, University of Nijmegen regarding Periodic Bond Chain theory, and Professor Jan Drenth of the Laboratory for Biophysical Chemistry, University of Groningen regarding the crystallographic structure of tetragonal lysozyme. The authors are also grateful to Mr Joel E. Adair of the Department of Chemical and Materials Engineering, University of Alabama in Huntsville for assistance in the construction of the crystal model.

References

Banerjee, S. K., Poglotti, A. & Rupley, J. A. (1975). *J. Biol. Chem.* **250**, 8260–8266.

Behlke, J. & Knespel, A. (1996). *J. Cryst. Growth*, **158**, 388–391.

Bennema, P. (1993). *Handbook of Crystal Growth*, Vol. 1, edited by D. T. J. Hurle, pp. 477–581. Amsterdam: North-Holland.

Bennema, P. & van der Eerden, J. P. (1987). *Morphology of Crystals*, edited by I. Sunagawa, pp. 1–75. Tokyo: Terra.
Blake, C. C. F., Johnson, L. N., Mair, G. A., North, A. C. T., Phillips, D. C. & Sarma, V. R. (1967). *Proc. R. Soc. London Ser. B*, **167**, 378–388.
Blake, C. C. F., Koenig, D. F., Mair, G. A., North, A. C. T., Phillips, D. C. & Sarma, V. R. (1965). *Nature (London)*, **206**, 757–761.
Blake, C. C. F., Mair, G. A., North, A. C. T., Phillips, D. C. & Sarma, V. R. (1967). *Proc. R. Soc. London Ser. B*, **167**, 365–377.
Boué, F., Lefaucheux, F., Robert, M. C. & Rosenman, I. (1993). *J. Cryst. Growth*, **133**, 246–254.
Brune, D. & Kim, S. (1994). *Proc. Natl Acad. Sci. USA*, **91**, 2930–2934.
Dao-Pin, S., Liao, D.-I. & Remington, S. J. (1989). *Proc. Natl Acad. Sci. USA*, **86**, 5361–5365.
Diamond, R. (1974). *J. Mol. Biol.* **82**, 371–391.
Durbin, S. D. & Carlson, W. E. (1992). *J. Cryst. Growth*, **122**, 71–79.
Durbin, S. D., Carlson, W. E. & Saros, M. T. (1993). *J. Phys. D*, **26**, B128–B132.
Durbin, S. D. & Feher, G. (1986). *J. Cryst. Growth*, **76**, 583–592.
Durbin, S. D. & Feher, G. (1990). *J. Mol. Biol.* **212**, 763–774.
Forsythe, E. & Pusey, M. L. (1994). *J. Cryst. Growth*, **139**, 89–94.
Frey, M., Genovesio-Taverne, J.-C. & Fontecilla-Camps, J. C. (1988). *J. Cryst. Growth*, **90**, 245–258.
Frey, M., Genovesio-Taverne, J.-C. & Fontecilla-Camps, J. C. (1992). *J. Phys. D*, **24**, 105–110.
Grubmüller, H., Heymann, B. & Tavan, P. (1996). *Science*, **271**, 997–999.
Hampe, O. G., Tondo, C. V. & Hasson-Voloch, A. (1982). *Biophys. J.* **40**, 77–82.
Hartman, P. (1987). *Morphology of Crystals*, edited by I. Sunagawa, pp. 269–319. Tokyo: Terra.
Hartman, P. & Perdok, W. G. (1955). *Acta Cryst.* **8**, 49–52, 521–524, 525–529.
Honig, B. & Nichols, A. (1995). *Science*, **268**, 1144–1149.
Honig, B., Sharp, K. & Yang, A. (1993). *J. Phys. Chem.* **97**, 1101–1109.
Imoto, T., Johnson, L. N., North, A. C. T., Phillips, D. C. & Rupley, J. A. (1972). *The Enzymes*, Vol. 7, edited by P. D. Boyer, pp. 665–808. New York: Academic Press.
Klapper, I., Hagstrom, R., Fine, R. M., Sharp, K. A. & Honig, B. (1986). *Proteins*, **1**, 47–59.
Kodandapani, R., Suresh, C. G. & Vijayan, M. (1990). *J. Biol. Chem.* **265**, 16126–16131.
Konnert, J. H., D'Antonio, P. & Ward, K. B. (1994). *Acta Cryst.* D**50**, 603–613.
Koppenol, W. H. (1981). *Oxygen and Oxy-Radicals in Chemistry and Biology*, edited by M. A. Rodgers & E. L. Powers, pp. 671–674. New York: Academic Press.
Li, M., Nadarajah, A. & Pusey, M. L. (1995). *J. Cryst. Growth*, **156**, 121–132.
Lim, K., Nadarajah, A. & Pusey, M. L. (1996). In preparation.
Luty, B. A., Wade, R. C., Madura, J. D., Davis, M. E., Briggs, J. M. & McCammon, J. A. (1993). *J. Phys. Chem.* **97**, 233–237.
Monaco, L.A. & Rosenberger, F. (1993). *J. Cryst. Growth*, **129**, 465–484.
Moult, J., Yonath, A., Traub, W., Smilansky, A., Podjarny, A., Rabinovich, D. & Saya, A. (1976). *J. Mol. Biol.* **100**, 179–195.
Nadarajah, A., Forsythe, E. L. & Pusey, M. L. (1995). *J. Cryst. Growth*, **151**, 163–172.
Nadarajah, A., Li, M. & Pusey, M. L. (1996). *J. Cryst. Growth*. Submitted.
Pusey, M. L. (1991). *J. Cryst. Growth*, **110**, 60–65.
Sharp, K., Fine, R. & Honig, B. (1987). *Science*, **236**, 1460–1463.
Sharp, K. A. & Honig, B. (1990). *Annu. Rev. Biophys. Biophys. Chem.* **19**, 301–332.
Sophianopoulos, A. J. (1969). *J. Biol. Chem.* **244**, 3188–3193.
Sophianopoulos, A. J. & Van Holde, K. E. (1964). *J. Biol. Chem.* **239**, 2516–2524.
Studebaker, J. F., Sykes, B. D. & Wien, R. (1971). *J. Am. Chem. Soc.* **93**, 4579–4585.
Wilcox, F. H. & Daniel, L. J. (1954). *Arch. Biochem. Biophys.* **52**, 305–312.
Wilson, L. J. & Pusey, M. L. (1992). *J. Cryst. Growth*, **122**, 8–13.
Zehavi, U. & Lustig, A. (1971). *Biochim. Biophys. Acta*, **236**, 127–130.